Regenerating vascular mural cells in zebrafish fin blood vessels are not derived from pre-existing ones and differentially require Pdgfrb signalling for their development

Leonard, E.V.; Figueroa, R.J.; Bussmann, J.; Lawson, N.D.; Amigo, J.D.; Siekmann, A.F.

Citation

Regenerating vascular mural cells in zebrafish fin blood vessels are not derived from pre-existing mural cells and differentially require Pdgfrb signalling for their development

Elvin V. Leonard[1,2], Ricardo J. Figueroa[3], Jeroen Bussmann[1,4], Nathan D. Lawson[5], Julio D. Amigo[3] and Arndt F. Siekmann[1,2,*]

ABSTRACT

Vascular networks comprise endothelial cells and mural cells, which include pericytes and smooth muscle cells. To elucidate the mechanisms controlling mural cell recruitment during development and tissue regeneration, we studied zebrafish caudal fin arteries. Mural cells colonizing arteries proximal to the body wrapped around them, whereas those in more distal regions extended protrusions along the proximo-distal vascular axis. Both cell populations expressed platelet-derived growth factor receptor β (*pdgfrb*) and the smooth muscle cell marker myosin heavy chain 11a (*myh11a*). Most wrapping cells in proximal locations additionally expressed actin alpha2, smooth muscle (*acta2*). Loss of Pdgfrb signalling specifically decreased mural cell numbers at the vascular front. Using lineage tracing, we demonstrate that precursor cells located in periarterial regions and expressing Pgdfrb can give rise to mural cells. Studying tissue regeneration, we did not find evidence that newly formed mural cells were derived from pre-existing cells. Together, our findings reveal conserved roles for Pdgfrb signalling in development and regeneration, and suggest a limited capacity of mural cells to self-renew or contribute to other cell types during tissue regeneration.

KEY WORDS: Zebrafish, Caudal fin, Blood vessel, Mural cell, Pdgfrb signalling, Tissue regeneration

INTRODUCTION

During tissue regeneration, lost cell types need to be replaced through *de novo* differentiation of tissue resident stem cells or from pre-existing differentiated cells (Poss, 2010). Several vertebrate species, such as zebrafish or newts, can regenerate a wide variety of tissues, such as appendages (Sehring and Weidinger, 2020; Tanaka, 2016), heart muscle (de Wit et al., 2020; González-Rosa et al., 2017; Xiang and Kikuchi, 2016) or retina (Alunni and Bally-Cuif, 2016; Wan and Goldman, 2016). By contrast, mammals have lost most of their regenerative potential and repair injured tissues through

imperfect wound healing, which can lead to scar formation and fibrosis (Eming et al., 2014; Erickson and Echeverri, 2018). During both processes, blood vessel regrowth occurs, highlighting their high regenerative potential (Chavez et al., 2016; DiPietro, 2013, 2016). However, it is not clear whether the newly formed blood vessels are equally functional in both settings, and how they might influence tissue regeneration. Blood vessels consist of endothelial cells lining the inner vessel surface and ensheathing mural cells. Studies in the zebrafish fin (Kametani et al., 2015; Tu and Johnson, 2011; Xu et al., 2014) and in mouse arteries (McDonald et al., 2018) have shown that endothelial cells in regenerating blood vessels are derived from pre-existing endothelial cells. Similarly, during wound healing, endothelial cells are being recruited from neighbouring blood vessels (Carmeliet, 2005; Tonnesen et al., 2000). These mechanisms closely resemble those observed during embryonic angiogenesis. By contrast, the ontogeny of newly forming murals cells and their contribution to blood vessel and tissue regeneration have remained unclear.

Mural cells can be subdivided into smooth muscle cells and pericytes, with intermediate cell types being present (Armulik et al., 2011; Grant et al., 2019; Holm et al., 2018). Generally, pericytes are important for guiding newly growing blood vessel sprouts during angiogenic phases (Eilken et al., 2017; Teichert et al., 2017) and later in blood vessel stabilization (Hellstrom et al., 2001). However, organ-dependent functional differences exist. In the brain, they ensure blood-brain barrier integrity (Langen et al., 2019) and regulate blood flow (Pfeiffer et al., 2021). Pericytes dying during an ischaemic attack have been implicated in preventing tissue reperfusion (Hall et al., 2014). Renal pericytes contribute to ultrafiltration and blood pressure control, while hepatic stellate cells regulate sinusoidal blood flow and have immunoregulatory properties (Holm et al., 2018). Several of these functions have been attributed to distinct mural cell shapes with smooth muscle cells showing a perpendicular wrapping morphology with respect to the blood vessel axis, while pericytes align longitudinally with this axis (Armulik et al., 2011; Holm et al., 2018). Mural cells furthermore display heterogeneity in their origins, with those in the head region being derived from neural crest (Sinha and Santoro, 2018). The mesothelium, which is the epithelium lining the coelomic cavity, generates most of the other mural cell populations with contributions from somitic tissue and the secondary heart field (Armulik et al., 2011). The degree to which these differences in origin contribute to functional differences between mural cells remains to be determined. One master regulator of mural cell development is platelet-derived growth factor β (Pdgfb) signalling (Kazlauskas, 2017). Mural cells and their progenitors express platelet-derived growth factor receptor β (*pdgfrb*), while endothelial cells express *pdgfb* ligands (Gaengel et al., 2009). Loss of *pdgfb* or

[1]Max Planck Institute for Molecular Biomedicine, Roentgenstr. 20, 48149 Münster, Germany. [2]Department of Cell and Developmental Biology, Perelman School of Medicine at the University of Pennsylvania, 1114 Biomedical Research Building, 421 Curie Boulevard, Philadelphia, PA 19104, USA. [3]Departamento de Fisiología, Facultad de Ciencias Biológicas, Pontificia Universidad Católica de Chile, Santiago, Chile. [4]Division of BioTherapeutics, Leiden Academic Centre for Drug Research (LACDR), Leiden University, PO Box 9502, 2300 RA Leiden, The Netherlands. [5]Department of Molecular, Cell and Cancer Biology, University of Massachusetts Medical School, 364 Plantation Street, Worcester, MA 01605, USA.

*Author for correspondence (arndt.siekmann@pennmedicine.upenn.edu)

N.D.L., 0000-0001-7788-9619; A.F.S., 0000-0001-6972-2173

pdgfrb results in a reduction of pericyte numbers in a tissue-specific manner without affecting their initial specification (Crosby et al., 1998; Hellstrom et al., 1999; Lindahl et al., 1997). Analysis of chimaeric animals suggests that smooth muscle cells similarly require *pdgfrb* signalling (Crosby et al., 1998). In zebrafish, mural cells can be detected along the trunk vasculature on the second day of development (Fortuna et al., 2015; Santoro et al., 2009), around 12 h after their appearance on the cranial vasculature (Ando et al., 2016; Wang et al., 2014). Studies addressing the origins of mural cells showed that trunk and hindbrain pericytes are mesoderm derived whereas those in more anterior regions have a neural crest origin (Ando et al., 2016; Stratman et al., 2017; Whitesell et al., 2014). Smooth muscle cells in zebrafish express similar marker genes when compared with mouse (Santoro et al., 2009), such as *tagln* (*SM22alpha*) (Li et al., 1996), *acta2* (Gabbiani et al., 1981) and *myh11* (Miano et al., 1994). A recent study also identified a conserved set of zebrafish pericyte genes (Shih et al., 2021). Zebrafish mural cells also require *pdgfrb* signalling during their development (Ando et al., 2021; Stratman et al., 2017). Together, these findings suggest that mural cell biology during developmental stages is well conserved in zebrafish.

Previous studies investigating mural cell function during tissue injury indicated that pericytes retained properties of mesenchymal stem cells with cultured pericytes being able to contribute an array of different cell types, such as chondrocytes (Crisan et al., 2008), adipocytes (Tang et al., 2008), skeletal muscle (Dellavalle et al., 2011, 2007) and neurons (Dore-Duffy et al., 2006). More recent results, however, showed that lineage-labelled pericytes did not contribute to these cell types in various injury settings *in vivo*, calling their stem cell properties into question (Guimaraes-Camboa et al., 2017). Despite these findings, work in zebrafish demonstrated that cells derived from *pdgfrb*-expressing mural cells contribute a specific extracellular matrix promoting axonal growth after spinal cord injury (Tsata et al., 2021). Studies examining mural cells during wound healing suggest that differentiated pericytes are activated and proliferate, subsequently supporting angiogenesis, while at other times promoting fibrosis (Ansell and Izeta, 2015; Rodrigues et al., 2019). Thus, the functional significance of pericytes during tissue regeneration remains an area of debate. In addition, studies unequivocally providing evidence concerning the origin of newly forming pericytes either during wound healing or tissue regeneration have been lacking (Rodrigues et al., 2019). We also lack an understanding of the signalling pathways that guide mural cell development during regeneration and how impaired mural cell function might impact the function of newly formed blood vessels and tissues.

Here, we have investigated mural cell morphology, ontogeny and the signalling pathways important for their development and regeneration in the zebrafish fin using newly developed transgenic lines. We show that zebrafish mural cells show two distinct morphologies depending on their proximo-distal location within the fin. They express the mammalian smooth muscle cell marker *myh11a* and can be lineage traced to tissue-resident progenitor cells. These express *pdgfrb*, but not *myh11a*. Furthermore, mural cell differentiation during both fin development and regeneration relies on Pdgfrb signalling. Lineage-tracing experiments, although not providing definite results, suggest that new perivascular cells in regenerating fins are not derived from pre-existing mural cells. We also do not detect significant contribution of differentiated mural cells to other cell types. Together, our studies illustrate the morphological diversity of mural cells in the zebrafish fin, while arguing against their stem cell properties. We further propose that the signalling mechanisms patterning mural cells during juvenile stages are being redeployed during tissue regeneration.

RESULTS

pdgfrb expression marks cells with distinct morphologies and anatomical locations within zebrafish fins

During juvenile stages, the fin vasculature expands ventrally from an artery-vein loop in the posterior part of the embryo and continues to grow during adulthood (Fig. 1A-E). To investigate mural cell development during these stages, we imaged double transgenic fish: *TgBAC(pdgfrb:citrine)*[s1010]; *Tg(-0.8flt1:RFP)*[hu5333]. In these animals, arterial ECs express red fluorescent protein (RFP), while *pdgfrb*-positive cells express citrine (Bussmann et al., 2010; Vanhollebeke et al., 2015). We observed the occurrence of citrine-expressing cells along the artery as early as 1 week post-fertilization (wpf; Fig. 1B,B′ white arrowheads). These cells were present throughout juvenile stages at 2 wpf (Fig. 1C-C″, white arrowheads) and 3 wpf (Fig. 1D,D′, white arrowheads), as well as in 4 wpf fish (Fig. 1E-H′). In addition to mural cells, we detected distinct cell types with varying levels of citrine expression. One population consisted of ovoid cells either located at the fin ray base (Fig. 1C′, yellow arrowheads) or at the bone ray joints at later developmental time points (Fig. 1G″, yellow arrowheads). Moreover, we found cuboidal-shaped cells surrounding arterial blood vessels (Fig. 1F-H′, pseudo-coloured in light green in Fig. 1G′,G″,H′). To characterize and quantify these distinct cell populations, we divided the fin into four segments (S1-S4), starting with S1 closest to the fish body towards S4 at the distal end of the fin. We then measured cellular dimensions and distribution throughout these segments. This analysis showed that, on average, citrine-expressing mural cells were longer and narrower than cuboidal-shaped cells (Fig. 1I). We also found that mural cell numbers increased from distal to more proximal locations (Fig. 1J). To examine mural cells more closely, we generated triple transgenic zebrafish: *TgBAC(pdgfrb:gal4)*[ncv24]; *Tg(UAS:GFP)*[nkuasgfp1a]; *Tg(-0.8flt:RFP)*[hu5333]. Analysis of these animals revealed additional morphological differences within the mural cell population. We found that GFP-expressing cells either wrapped around arteries (Fig. S1A-C′, Movies 1 and 2) or sent out long protrusions along the vessel axis (Fig. S1D-E′, red arrowheads, see also Fig. 1G-H′, Movies 3 and 4). These cells were differentially distributed along the proximo-distal fin axis. Although S4 was mostly devoid of mural cells, S3 contained mainly mural cells with long protrusions. Mural cells in segments closer to the body (S1 and S2) were characterized by their wrapping morphology (Fig. 1K). To further characterize these morphologies, we made use of a double transgenic approach using *TgBAC(pdgfrb:gal4)*[ncv24]; *Tg(UAS:KAEDE)*[s1999t] fish. These fish express the photoconvertible protein Kaede in mural cell populations. Kaede photoconversion revealed complex cell shapes consisting of numerous finger-like extensions surrounding arteries (Fig. 1L,M, Movies 5 and 6). Wrapping mural cells either showed distinct borders between each other or overlapped (Fig. 1L,M). Thus, using citrine expression, as well as cell shapes as defining criteria, we were able to distinguish at least four different populations of *pdgfrb*-expressing cells in developing zebrafish fins.

Co-expression of *pdgfrb* and *myh11a* defines the mural cell populations

The classical perception of mural cell distribution along the vascular tree posits that proximal arterioles are covered by smooth muscle cells with their distinct morphologies surrounding arteries with their
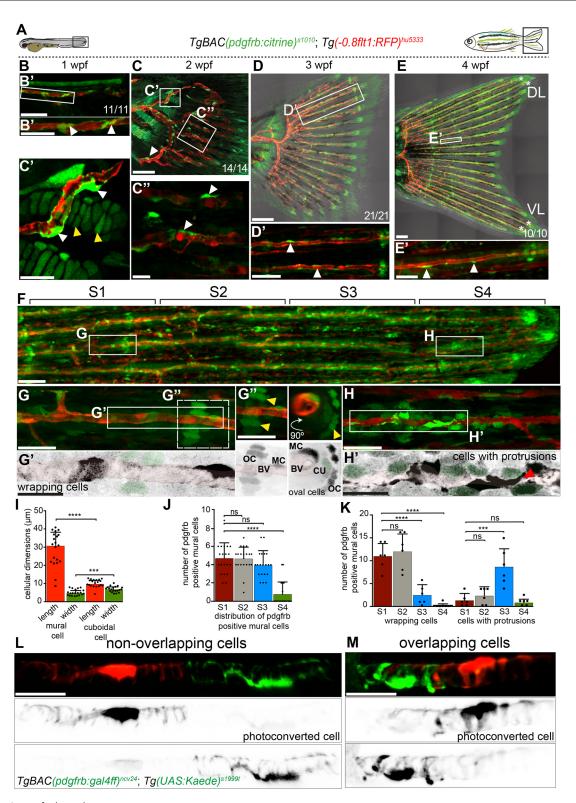
Fig. 1. See next page for legend.

entire cell bodies, while more distally located capillaries are ensheathed by pericytes (Grant et al., 2019; Holm et al., 2018). Based on this, we hypothesized that the mural cells we detected in distal segments of the fin most likely resembled pericytes, but we were unsure to what extent wrapping cells in more proximal locations would be similar to smooth muscle cells. To further

investigate these identities, we developed a transgenic line expressing yellow fluorescent protein (YFP) under the control of the myosin heavy chain 11a (*myh11a*) promoter, a gene reported to be smooth muscle cell specific (Miano et al., 1994; Vanlandewijck et al., 2018). Accordingly, when analysing double transgenic *Tg(0.8flt1:RFP)*[hu5333]; *TgBAC(myh11a:YFP)*[mu125] zebrafish

Fig. 1. Pdgfrb expression marks distinct cell populations in developing zebrafish fins. Maximum intensity projections of confocal *z*-stacks of *TgBAC(pdgfrb:citrine)*^{s1010}; *Tg(-0.8flt1:RFP)*^{hu5333} double transgenic fish labelling arterial ECs (red) and *pdgfrb*-positive cells (green) in lateral views with anterior towards the left. (A) Schematic representation of time course of the study (1 to 4 wpf). (B) Citrine-expressing cells colonize axial vessels at 1 wpf. Scale bar: 20 μm. (B′) The outlined area in B showing association of mural cells with arteries (white arrowheads). Scale bar: 10 μm. (C) Citrine-expressing cells at 2 wpf. Scale bar: 30 μm. (C,C″) The outlined areas in C show the association of individual mural cells with arteries (white arrowheads). Clusters of oval shaped cells at 2 wpf are indicated (yellow arrowheads, C″). Scale bar: 10 μm. (D) Vasculature at 3 wpf. Scale bar: 70 μm. The outlined area enlarged in D′ shows the association of citrine-expressing cells (white arrowheads) with arteries. Scale bar: 15 μm. (E) Caudal fin vasculature at 4 wpf; asterisks indicate the four blood vessels used for quantification. DL, dorsal fin lobe; VL, ventral fin lobe. Scale bar: 100 μm. The outlined area enlarged in E′ shows citrine-expressing cells along arteries (white arrowheads). Scale bar: 30 μm. Numbers represent individual animals analysed. (F) Caudal fin at 4 wpf. Scale bar: 20 μm. S1-S4 represent segments used for quantification. (G) Proximal segment. Scale bar: 10 μm. The area indicated by a solid outline is enlarged in G′ and shows citrine-expressing cells wrapping around blood vessels. Scale bar: 7 μm. The area indicated by a dashed outline is enlarged in G″ and shows citrine-expressing mural cells (MCs) on blood vessels (BVs), oval shaped cells (OCs) surrounding vessels (yellow arrowheads) and citrine-expressing cuboidal-shaped cells (CUs, pseudo-coloured in green) between the mural cells and oval-shaped cells. Scale bar: 5 μm. (H) Distal segment of caudal fin blood vessel. Scale bar: 10 μm. The outlined area enlarged in H′ shows citrine-expressing cells with protrusions (red arrowhead). Citrine-expressing cuboidal cells are highlighted in green. Scale bar: 7 μm. (I) Classification of citrine-expressing cells based on their dimensions. Mann-Whitney test, *n*=20 for each cell type. ***P*=0.0001, ****P*≤0.0001. (J) Quantification of citrine-expressing mural cells across segments. One-way ANOVA [*n*=20 caudal fin arteries from five different fish (average size 1194 μm)]. ****P*≤0.0001. (K) Quantification of cell morphologies of *TgBAC(pdgfrb:gal4ff)*^{ncv24}; *Tg(UAS:GFP)*^{nkuasgfp1a}-expressing cells. One-way ANOVA [*n*=12 caudal fin arteries from six individual fish (average length 1673 μm)]. ***P*≤0.0002, ****P*≤0.0001. (L,M) Maximum intensity projections of confocal *z*-stacks of *TgBAC(pdgfrb:gal4ff)*^{s1999}; *Tg(UAS:Kaede)*^{ncv24} mural cells. Non-overlapping cells (L) and overlapping cells (M). Scale bars: 10 μm.

embryos at 5 days post fertilization (dpf), we detected YFP expression in mural cells surrounding arteries and in circulation (Fig. S2A-C). Prominent YFP expression was also detectable in gut smooth muscle cells (Fig. S2A, arrows). Similar to *Tg(pdgfrb: citrine)*^{s1010} fish, we detected YFP-expressing cells ensheathing fin arteries as early as 1 wpf (Fig. S2D-E′, yellow arrowheads) and throughout juvenile stages up to 4 wpf (Fig. S2F-H′, yellow arrowheads). We then quantified their morphology and distribution along the proximo-distal axis in 4 wpf larvae (Fig. 2A-F). This analysis revealed a striking similarity with respect to their distribution when compared with citrine-expressing mural cells in *TgBAC(pdgfrb:citrine)*^{s1010} fish. We detected both, wrapping cells (Fig. 2B,B′) and cells with protrusions (Fig. 2C,C′, red arrowheads) expressing YFP. A greater number of cells displayed wrapping morphology in proximal regions, whereas more distal regions contained mostly cells exhibiting protrusions (Fig. 2D,D′, red arrowhead). The most distal segment (S4) was again mostly devoid of mural cells (Fig. 2F). Thus, in the zebrafish fin, mural cells without a characteristic smooth muscle cell morphology also express YFP driven by the *myh11a* promoter.
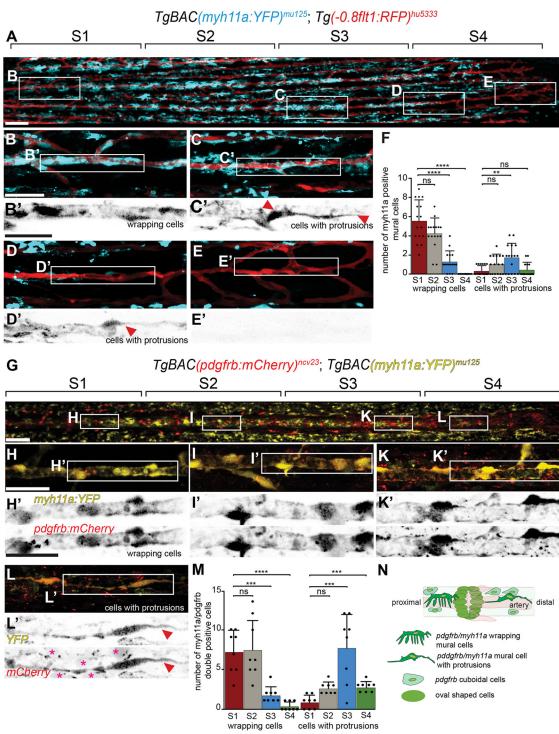
To determine the relationship between *pdgfrb*- and *myh11a*-expressing cells, we generated double transgenic animals *TgBAC(pdgfrb:mCherry)*^{ncv23}; *TgBAC(myh11a:YFP)*^{mu125}, expressing mCherry under the control of the *pdgfrb* promoter and YFP in *myh11a*-positive cells (Fig. 2G-L). All YFP-expressing mural cells examined were positive for both transgenes. By contrast, mCherry-expressing cuboidal cells did not express YFP (Fig. 2L′,

magenta asterisks). We again detected a higher number of wrapping double-positive cells in proximal fin regions, whereas distal fin regions mostly contained cells with protrusions (Fig. 2M). To determine whether *pdgfrb* and *myh11a* co-expression was a specific feature of fin mural cells, we analysed mural cells in the trunk of embryonic zebrafish at 6 dpf (Fig. S3A-E). In this setting, we found *pdgfrb*-expressing mural cells on both arterial and venous intersegmental vessels (ISVs). A greater number of mural cells on arterial ISVs also expressed the *myh11a* transgene when compared with venous ISVs, while mural cells only expressing *pdgfrb* were more abundant on venous ISVs. Together, these findings reveal that distinct mural cell morphologies in the zebrafish fin do not correlate with differences in the expression of the contractile protein Myh11a. Our findings further show that *pdgfrb* is more broadly expressed when compared with *myh11a* (Fig. 2N).

Acta2 expression distinguishes mural cells in proximal fin regions and negatively correlates with Notch signalling pathway activation

As *pdgfrb* and *myh11a* were surprisingly expressed in all mural cell populations, we sought to identify markers that would label different subsets of fin mural cells. *Acta2* is a known smooth muscle cell marker both in mice (Gabbiani et al., 1981) and zebrafish (Whitesell et al., 2014). We combined *Tg(acta2:mCherry)*^{ca8} with *TgBAC(myh11a:YFP)*^{mu125} fish and analysed fluorescent protein expression in their progeny. At embryonic stages, we found distinct and overlapping expression domains of these two transgenes (Fig. S3F-H). The outflow tract of the heart showed *myh11a* expression, while the ventricle was expressing *acta2* (Fig. S3G). In intersegmental vessels, we detected both transgenes in mural cells on arteries (Fig. S3H). We then analysed the fin vasculature at 4 wpf (Fig. 3A-D) and at 6 wpf (Fig. 3E-H). This analysis revealed the existence of *acta2/myh11a* double-positive mural cells on proximally located arteries, while *acta2* expression was absent in more distal regions of the fin (Fig. 3D,H). Thus, mural cells with elongated morphology do not express *acta2*, while wrapping cells can express either *myh11a* or *myh11a* together with *acta2*. These findings illuminate morphological and gene expression differences within mural cells of the zebrafish fin. They furthermore suggest that the previously established proximo-distal hierarchy in terms of smooth muscle cell to pericyte transition along the vascular tree is conserved in the zebrafish fin. We thus define those fin mural cells that express *acta2*, *myh11a* and *pdgfrb* and exhibit a wrapping morphology as smooth muscle cells. Mural cells expressing *myh11a* together with *pdgfrb* and showing an elongated morphology, we define as pericytes. Cells with wrapping morphology displaying *myh11a* and *pdgfrb* expression, but no *acta2* expression might constitute an intermediate mural cell population.

Notch signalling is implicated in regulating mural cell specification (Ando et al., 2016) and proliferation (Wang et al., 2014). We therefore asked whether we might observe differences in Notch signalling pathway activation in different mural cell populations. Analysis of *Tg(TP1bglob:VenusPEST)*^{s940}; *Tg(acta2: mCherry)*^{ca8} animals revealed Notch pathway activation (indicated through venusPEST expression) predominantly in mural cells in distal fin regions, whereas *acta2*-expressing mural cells were mostly devoid of notch pathway activation (Fig. 3I-L). We also analysed the overlap of *pdgfrb* expression with Notch pathway activation using *TgBAC(pdgfrb:gal4ff)*^{ncv24}; *Tg(UAS:GFP)*^{nkuasgfp1a}; *Tg(TP1bglobin:H2B-mCherry)*^{s939} animals (Fig. S4). This analysis revealed Notch pathway activation in *pdgfrb*-expressing mural cells in distal fin regions, while in more proximal fin regions, we detected

Fig. 2. Co-expression of *myh11a* and *pdgfrb* distinguishes vascular mural cells from other *pdgfrb*-expressing cell populations. Maximum intensity projections of confocal *z*-stacks of *Tg(-0.8flt1:RFP)*[hu5333]; *TgBAC(myh11a:YFP)*[mu125] double transgenic fish labelling arterial ECs (red) and YFP-positive cells (blue); lateral views, anterior towards the left. (A) Caudal fin of 4 wpf fish. Scale bar: 100 µm. S1-S4 represent the four segments used for quantifying the distribution of YFP-expressing cells. Areas shown enlarged in B-E are indicated. (B) Proximal segment. Scale bar: 10 µm. (B′) The area outlined in B showing YFP-positive cells wrapping around blood vessels. (C-E) Mid-vessel and distal segments of a caudal fin blood vessel. The outlined areas are enlarged in C′-E′. Scale bar: in B′, 7 µm for B′-E′. (F) Quantification of YFP-positive cell distribution. One-way ANOVA [*n*=16 caudal fin arteries from 8 individual fish (average length: 1006 µm)]. **P=<0.0012, ****P=<0.0001, n.s., not significant. Data are mean±s.d. (G) Maximum intensity projections of confocal *z*-stacks of *TgBAC(pdgfrb:mCherry)*[ncv23]; *TgBAC(myh11a:YFP)*[mu125] double transgenic fish in lateral views with anterior towards the left. Caudal fin of 4 wpf fish. Scale bar: 100 µm. S1-S4 represent the four segments used for quantification. (H-L) Proximal (H), mid-vessel (I) and distal (K,L) segments of double transgenic fish. Scale bar: 10 µm. (H′-L′) The areas outlined in H-L showing the overlap of mCherry and YFP fluorophores (L′, red arrowheads). Cuboidal cells express only *pdgfrb:mCherry* (L′, magenta asterisks). Scale bar: 10 µm. (M) Quantification of the distribution of *myh11a/pdgfrb*-positive cells. One-way ANOVA [*n*=8 caudal fin arteries from 5 individual fish (average length:1938 µm)]. ***P≤0.000, ****P≤0.0001; n.s., not significant. Data are mean±s.d. (N) Schematic illustrating the distribution of different fin cell populations.
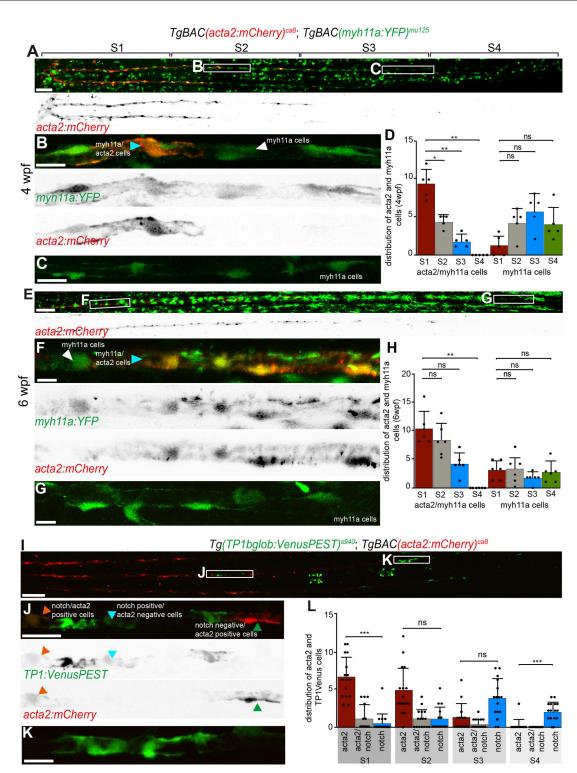
Fig. 3. Differential Notch signalling coincides with *acta2* expression along the proximo-distal axis. (A-C,E-G) Maximum intensity projections of confocal *z*-stacks of *TgBAC(acta2:mCherry)^{ca8}; TgBAC(myh11a:YFP)^{mu125}* fins, labelling *myh11a*-positive cells (green) and *acta2*-positive cells (red). (A) Caudal fin of 4 wpf fish. Scale bar: 80 µm. (B) Mural cells expressing *myh11a* (white arrowheads) or *myh11a/acta2* (blue arrowheads). Scale bar: 5 µm. (C) Mural cells in distal region. Scale bar: 5 µm. (D) Distribution of *myh11a* and *myh11a/acta2* double-positive cells along proximal and distal segments. One-way ANOVA [*n*=5 fin rays from three different fish (average length: 1707 µm)]. *P=0.0355, **P=0.0072, n.s., not significant. Data are mean±s.d. Individual data points represent individual fin rays. (E) Caudal fin of 6 wpf fish. Scale bar: 100 µm. (F) Mural cell expressing *myh11a* (white arrowhead) or *myh11a/acta2* (blue arrowhead). Scale bar: 10 µm. (G) Mural cells in distal regions express only *myh11a*. Scale bar: 10 µm. (H) Distribution of *myh11a* and *myh11a/acta2*-positive cells. One-way ANOVA [*n*=6 fin rays from six different fish (average length: 2381 µm)]. **P=0.0039, n.s., not significant. Data are mean±s.d. Individual data points represent individual fin rays. (I-K) Maximum intensity projections of *TgBAC(acta2:mCherry)^{ca8}; Tg(TP1bglob:VenusPEST)^{s940}* fins, labelling *acta2*-positive cells (red) and those with activated notch signaling (green). (I) Caudal fin of 4 wpf fish. Scale bar: 70 µm. (J) *notch* positive/*acta2* negative (blue arrowheads); *notch* negative/*acta2* positive (green arrowheads); *notch* positive/*acta2* positive (orange arrowheads). Scale bar: 10 µm. (K) Mural cell in distal segment. Scale bar: 5 µm. (L) Distribution of *acta2* and cells with *notch* pathway activation. One-way ANOVA [*n*=16 fin rays from five different fish (average length: 1947 µm)]. n.s., not significant; ***P<0.0006. Data are mean±s.d.
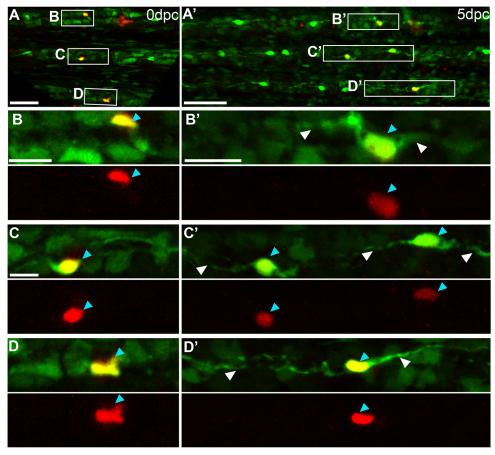
pdgfrb-positive cells that did not exhibit notch pathway activity. Thus, pericytes in distal fin regions show Notch pathway activation, whereas smooth muscle cells in more proximal regions do not.

pdgfrb-expressing cuboidal-shaped cells are precursors for vascular mural cells

We then set out to determine the cell population giving rise to fin mural cells. To do so, we generated transgenic fish that express the photoconvertible Dendra2 protein in the nuclei of *pdgfrb*-positive cells: *TgBAC(pdgfrb:H2B-dendra2)^{mu158}* (Fig. S5A-D). Proof of concept studies in embryos showed that Dendra2 was expressed in mural cell populations in different embryonic regions (Fig. S5B′-D, white arrowheads) and could be photoconverted upon blue light exposure (Fig. S5B′-D, blue arrowheads). Based on their location close to arteries, we focused on cuboidal-shaped cells as potential mural cell precursors. To examine possible changes

in cell shapes, we crossed *TgBAC(pdgfrb:H2B-dendra2)^{mu158}* fish with *TgBAC(pdgfrb:gal4ff)^{ncv24}; Tg(UAS:EGFP)^{nkuasgfp1a}* fish, expressing cytoplasmatic EGFP in *pdgfrb*-positive cells. Examination of individual photoconverted cuboidal cells 5 days post-photoconversion (dpc; Fig. 4) revealed that a proportion of photoconverted cells had undergone cell shape changes, now extending long processes along the vessel axis. As we did not photoconvert single cells, we analysed how many photoconverted cells transitioned towards the mural cell lineage. This analysis revealed that most cells maintained their cuboidal morphology after photoconversion (Fig. 4E-G). These results suggest that fin mural cells can differentiate from local precursors that express *pdgfrb*.
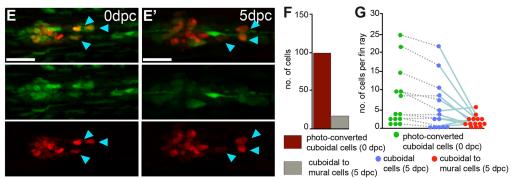
Previous studies showed that *col1a2* expressing fibroblasts can give rise to pericytes during embryonic development (Rajan et al., 2020). We therefore asked whether cuboidal-shaped cells belonged to the fibroblast lineage. To do so, we used a transgenic line expressing

TgBAC(pdgfrb:gal4ff)^{ncv24}; Tg(UAS:GFP)^{nkuasgfp1a}; TgBAC(pdgfrb:H2B-dendra2)^{mu158}

Fig. 4. Cuboidal and *pdgfrb*-expressing cells differentiate into mural cells during caudal fin artery development. Maximum intensity projections of confocal z-stacks of *TgBAC(pdgfrb:gal4ff)^{ncv24tg}); Tg(UAS: GFP)^{nkuasgfp1a}; TgBAC(pdgfrb:H2B-dendra2)^{mu158}* fins, labelling *pdgfrb*-positive cells (green). (A,A′) Photoconverted nuclei at 0 and 5 dpc. Scale bars: 20 μm in A; 30 μm in A′. The outlined areas enlarged in B-D show photoconverted individual cells (blue arrowheads) at 0 dpc. Scale bars: in B, 15 μm for B; in C, 20 μm for C,D. The outlined areas enlarged in B′-D′ shows photoconverted cells (blue arrowheads) extending protrusions (white arrowheads). Scale bar: 20 μm. (E,E′) Photoconverted nuclei at 0 and 5 dpc (blue arrowheads). Scale bars: 20 μm. (F) Total number of photoconverted cells at 0 dpc and photoconverted cells extending protrusions at 5 dpc. (G) Number of photoconverted cuboidal cells at 0 dpc (green circle), cells that remained cuboidal (blue circle) and cells that extended protrusions (red circle) at 5 dpc. Data represent number of individual cells photoconverted per fin ray (14 fin rays) from *n*=8 individual fish.

GFP under the control of the *col1a2* promoter (Rajan et al., 2020) and analysed GFP expression in the fin. Mural cells in proximal fin regions only expressed *pdgfrb*, while we detected *col1a2* expression in cuboidal-shaped cells (Fig. 5A,B). In middle regions of the fin, double positive cells of cuboidal morphology were readily detectable (Fig. 5C). Mural cells did not show *col1a2* expression in this fin region, either. In most distal regions, we found double positive cells of cuboidal (Fig. 5D,E, red arrowheads) and mural cell morphology (Fig. 5D,E, blue arrowheads). To further investigate these changes, we sorted mural cells based on their co-expression of *pdgfrb* and *myh11a* and single *pdgfrb* expressing cells from zebrafish fins and compared the expression patterns of fibroblast and mural cell genes (Fig. 5F,G). Double positive cells showed an upregulation of mural cell markers, while trending towards a decrease in fibroblast markers when compared to single *pdgfrb* expressing cells (Fig. 5G). Thus, like in embryonic zebrafish, mural cells in the fins of juvenile zebrafish might be partially derived from cells of fibroblastic origin, which downregulate fibroblast markers during their maturation.

Fin mural cell development in juvenile stages requires *pdgfrb* signalling

To determine the signalling pathways required for fin mural cell differentiation, we examined *pdgfrb*^{um148} mutant zebrafish

(Kok et al., 2015). We again divided fin arteries into four segments and quantified the distribution of mural cells using *TgBAC(pdgfrb:gal4)*^{ncv24}; *Tg(UAS:GFP)*^{nkuasgfp1a}; *Tg(-0.8flt1:RFP)*^{hu5333} transgenic animals. In wild-type siblings, we observed a decrease of mural cell numbers along the proximo-distal fin axis (Fig. 6A-C′, yellow arrowheads, quantified in Fig. 6G). Cuboidal cells were more homogenously distributed (Fig. 6B′,C′, segments S3 and S4, blue arrowheads, quantified in Fig. 6H). In *pdgfrb*^{um148} mutant fish (Fig. 6D-F′), we observed only a small reduction in mural cell numbers in proximal segments (Fig. 6E,E′, yellow arrowheads, quantified in Fig. 6G, Movies 7 and 8), whereas those in distal segments were strongly decreased (Fig. 6F,F′, quantified in Fig. 6G). Of interest, cuboidal cells in distal fin regions increased in number in mutant animals (Fig. 6F,F′, blue arrowheads, quantified in Fig. 6H, Movies 9 and 10). To corroborate our findings, we also analysed the distribution of mural cells in *TgBAC(pdgfrb:citrine)*^{s1010}; *Tg(-0.8flt1:RFP)*^{hu5333} and *TgBAC(myh11a:YFP)*^{mu125}; *Tg(-0.8flt1:RFP)*^{hu5333} fish (Fig. S6). We detected a similar change in mural/cuboidal cell distribution in these transgenic fish and additionally observed an increase in citrine expression levels in cuboidal cells in *pdgfrb*^{um148} mutants (Fig. S6K). This suggests a block in differentiation of cuboidal-shaped cells into the mural cell lineage in *pdgfrb*^{um148} mutants,
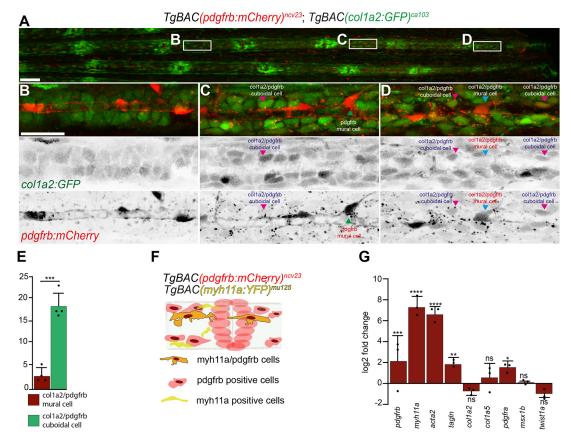

Fig. 5. Expression of *pdgfrb* and *col1a2* in cuboidal and mural cells. Maximum intensity projections of confocal *z*-stacks of *TgBAC(pdgfrb:mCherry)*^{ncv23}; *TgBAC(col1a2:GFP)*^{ca103} fins, labelling *pdgfrb*-positive cells (red) and *col1a2*-positive cells (green). (A-D) Caudal fin of 4 wpf fish. Scale bar: 100 µm for A. (B) Mural cells in the proximal segments express only *pdgfrb* and no *col1a2*. Scale bar: 7 µm. (C) Cuboidal cells express both *pdgfrb* and *col1a2* (magenta arrowheads), while mural cell express only *pdgfrb* (green arrowheads). (D) Distal segments contain mural cells (blue arrowheads) and cuboidal cells (magenta arrowheads) expressing both *pdgfrb* and *col1a2*. (E) Number of cuboidal and mural cells in D. Unpaired *t*-test. ***P=0.0029, n=4 different fish. Individual data points represent individual fin rays. (F) Schematic representation of cell types labelled in caudal fin of *TgBAC(pdgfrb:mCherry)*^{ncv23}; *TgBAC(myh11a:YFP)*^{mu125} double transgenic fish. (G) Relative expression of genes in *pdgfrb*/*myh11a* (RFP/YFP) positive cells compared with expression in *pdgfrb* only (RFP)-expressing cells was set as 1 (or 0 in log2 fold change). Individual data points represent log2 fold change, from independent experiments; dCt values from independent experiments was used to calculate significance. One-way ANOVA. n.s., not significant; *P= 0.0177, **P≤0.0032, ***P≤0.0005, ****P≤0.0001. Data are mean±s.d.
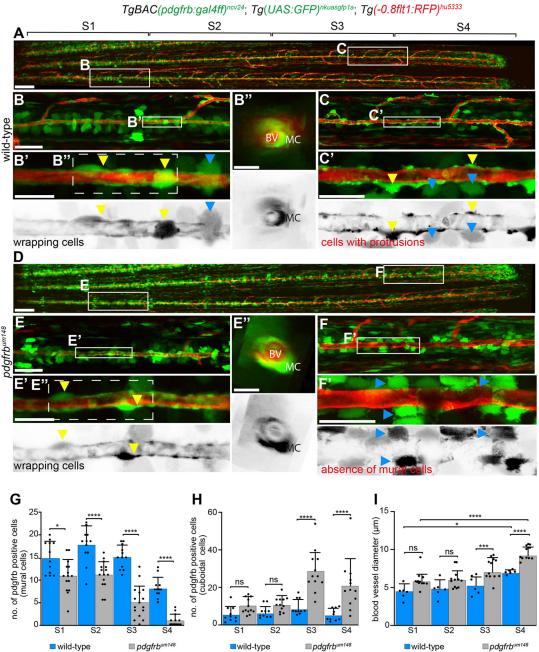
Fig. 6. Mural cell recruitment to caudal fin arteries requires Pdgfrb signalling. Maximum intensity projections of confocal *z*-stacks of *TgBAC(pdgfrb: gal4ff)*[ncv24tg]; *Tg(UAS:GFP)*[nkuasgfp1a]; *Tg(-0.8flt1:RFP)*[hu5333] fish. (A) Caudal fin artery in wild-type fish at 5 wpf. Scale bar: 100 μm. (B,C) Proximal and distal segments. Scale bar: 10 μm. (B′,C′) The outlined areas in B,C showing mural (yellow arrowheads) and cuboidal (blue arrowheads) cells. Scale bar: 3 μm. (B″) The outlined area in B′ showing mural cells in proximal regions. Scale bar: 3 μm. (D) Caudal fin vessel in *pdgfrb*[um148] mutant fish at 5 wpf. Scale bar: 100 μm. (E,F) Proximal and distal segments. Scale bar: 10 μm. (E′,F′) The outlined areas in E,F showing mural (yellow arrowheads) and cuboidal (blue arrowheads) cells. Scale bar: 3 μm. (E″) The outlined area in E′ showing mural cells wrapping around artery. Scale bar: 3 μm (G) Quantification of mural cell distribution across fin segments in wild-type and *pdgfrb*[um148] fish. One-way ANOVA. *n*=12 fin rays from six different fish for wild type (average length: 2509 μm), *n*=15 fin rays from eight different fish for mutant (average length: 2377 μm). n.s., not significant; *P=0.0215, ****P=<0.0001. Data are mean±s.d. Individual data points represent individual fin rays. (H) Quantification of cuboidal cells in wild-type and *pdgfrb*[um148] fish. One-way ANOVA. *n*=10 fin rays from six different fish for wild type, *n*=12 fin rays from six different fish for mutant. n.s., not significant; ****P≤0.0001. Data are mean±s.d. Individual data points represent individual fin rays. (I) Artery diameter along the proximal distal axis in wild-type and *pdgfrb*[um148] fish; mutant fish display dilated vessels. One-way ANOVA. *n*=6 fin rays from six different fish for wild type, *n*=12 fin rays from six different fish for mutant. n.s., not significant; *P≤0.0132, ***P=0.0005, ****P≤0.0001. Data are mean±s.d. Individual data points represent individual fin rays.

while at the same time leading to an upregulation of *pdgfrb* promoter activity in this precursor lineage. Therefore, also in the zebrafish fin, Pdgfrb signalling is instrumental for proper mural cell specification. However, proximal blood vessel segments were still ensheathed with mural cells expressing transgenes driven by both *pdgfrb* and *myh11a* promoters. This resembles early larval stages, where some smooth muscle cell populations also appear unaffected in *pdgfrb*[um148] mutants (Ando et al., 2021).

We then determined possible changes in vascular function in *pdgfrb*[um148] mutants. To do so, we measured blood vessel diameters along the proximo-distal fin axis. This analysis revealed an increase in blood vessel diameters in distal segments in mutant animals (Fig. 6I). This indicates that, similar to mice (Hellstrom et al., 2001) and zebrafish brain blood vessels (Ando et al., 2021), loss of mural cells in *pdgfrb*[um148] mutant animals results in fin blood vessel dilation.

Regenerating fin mural cells require *pdgfrb* signalling

To examine whether the same signals contribute to mural cell development in tissue regeneration, we performed two types of fin regeneration experiments in wild-type and *pdgfrb*[um148] mutant animals. We either removed a piece of tissue containing a bone ray and an artery in the centre of a fin ray (Fig. 7A), or amputated about 50% of the fin (Fig. S7). We then allowed the tissue to regenerate and determined mural cell numbers. In wild-type fish, we observed a newly forming artery as early as 3 days post-injury (dpi; Fig. 7B,C), with a fully regenerated artery ensheathed by mural cells being present at 5 dpi (Fig. 7D-F). When comparing wild-type fish (Fig. 7G-I,M) at 7 dpi to *pdgfrb*[um148] mutants, we observed a significant reduction in mural cell recruitment to the artery in mutants (Fig. 7J-M). We also detected a reduction in mural cell coverage around regenerated arteries in the fin amputation assay, both in *TgBAC(pdgfrb:citrine)*[s1010] (Fig. S7A-D′) and in *TgBAC(myh11a:YFP)*[mu125] transgenic animals (Fig. S7E-H′, quantified in I). Although these defects did not lead to a reduction of regenerate outgrowth (Fig. S8A-C), we observed an increase in connections between regenerated arteries and veins in *pdgfrb*[um148] mutant fish (Fig. S8A′,B′, red asterisks, quantified in D). Thus, also
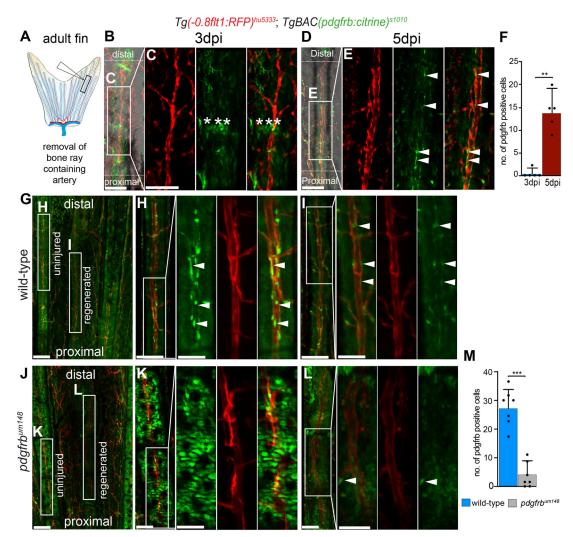

Fig. 7. Pdgfrb signalling regulates mural cell recruitment during fin regeneration. (A) Schematic representation of experimental approach to study blood vessel growth in regenerating tissue. Maximum intensity projections of *TgBAC(pdgfrb:citrine)*[s1010]; *Tg(-0.8flt1:RFP)*[hu5333] fish. (B) Regenerating fin at 3 dpi. Scale bar: 50 μm. (C) Citrine-positive oval cells (asterisks). Scale bar: 30 μm. (D,E) Recruitment of mural cells (arrowheads). Scale bar: 50 μm. (F) Quantification of mural cells. Mann-Whitney test, *n*=5 fish for each time point. n.s., not significant; Data are mean±s.d. **P=0.0079. (G) Mural cell recruitment in wild-type fish. Scale bar: 50 μm. (H) Uninjured bone segment of wild-type fish. Scale bar: 20 μm. The outlined area is enlarged on the right showing mural cells (white arrowheads). Scale bar: 8 μm. (I) Regenerated bone segment at 7 dpi. Scale bar: 20 μm. The outlined area is enlarged on the right showing mural cells (white arrowheads). Scale bar: 8 μm. (J) Mural cell recruitment in *pdgfrb*[um148] mutant fish. Scale bar: 50 μm (K) Uninjured bone segment. Scale bar: 20 μm. The outlined area is enlarged on the right showing cuboidal cells. Scale bar: 8 μm (L) Regenerated bone segment at 7 dpi. Scale bar: 20 μm. The outlined area is enlarged on the right showing a decrease in mural cells (white arrowheads). Scale bar: 8 μm. (M) Quantification of mural cell numbers in wild-type and *pdgfrb*[um148] fish. Mann–Whitney test, *n*=7 fish. Data are mean±s.d. ***P=0.0006.

in regenerative settings, *pdgfrb* signalling is a prerequisite for proper mural cell differentiation. These findings suggest that developmental signals are re-used during mural cell specification in regenerating tissues.

Pre-existing mural cells are not precursors for regenerating mural cells

During regeneration, either tissue-resident stem stells or dedifferentiated lineage-restricted precursor cells are the source for new tissues and cell types (Tanaka and Reddien, 2011). To analyse whether new mural cells are derived from pre-existing ones, we tracked mural cells during regeneration through photoconverting Dendra2 protein in cells around the injury site in *TgBAC(pdgfrb: H2B-dendra2)*[mu158] fish (Fig. 8A-C). We then determined the contribution of photoconverted mural cells to the newly formed tissue at 5 dpi (Fig. 8D,E). We exclusively detected newly made

green Dendra2 protein in the regenerated region of the fin, while the surrounding tissue still contained an abundance of previously photoconverted red cells (Fig. 8E).

As transgenic lines can show mosaicism and not all Dendra2-expressing cells might be photoconverted in our experiments, we sought to verify our lineage-tracing results using an alternative approach. We decided to directly image mural cells on blood vessels next to generating arteries on consecutive days (Fig. 9). This analysis revealed only subtle changes in the location of pre-existing mural cells on uninjured blood vessels (Fig. 9A), while we readily detected the emergence of new mural cells on nascent arteries (Fig. 9A, day 5-7, asterisks). We also analysed whether newly forming cuboidal cells would give rise to regenerating mural cells, as we had observed in growing fins. Examination of *TgBAC(pdgfrb:mcherry)*[ncv23]; *TgBAC(col1a2)*[ca103] fish indeed showed the existence of cells expressing both transgenes at early
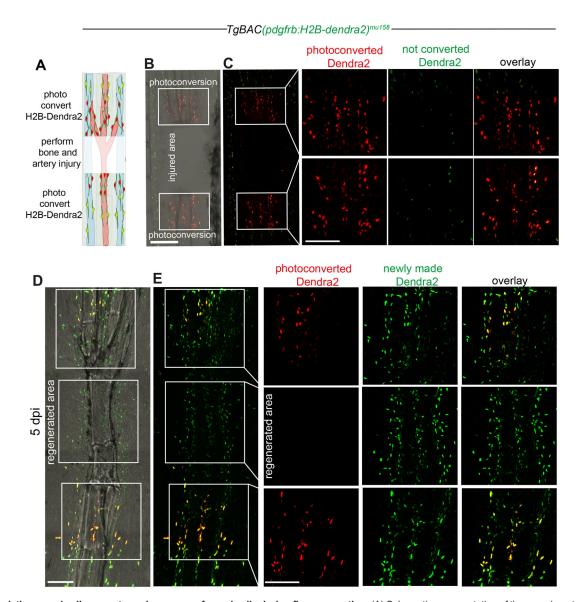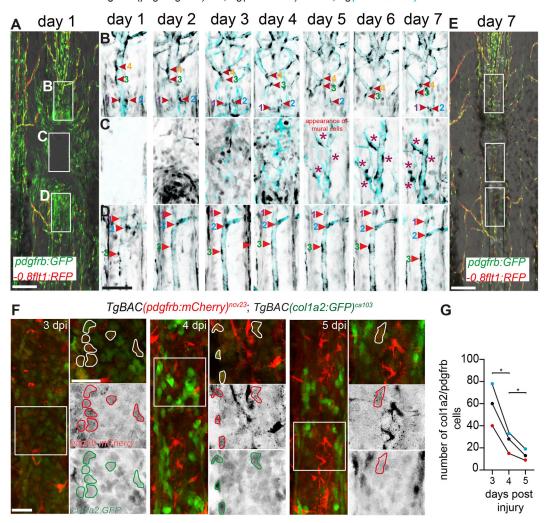

Fig. 8. Pre-existing mural cells are not a major source of mural cells during fin regeneration. (A) Schematic representation of the experimental approach to study fin regeneration. Maximum intensity projections of *TgBAC(pdgfrb:H2B-dendra2)*[mu158]. (B) Fin ray 12 hpi. Green to red photoconversion was performed above and below the site of injury. Scale bar: 100 µm. (C) Photoconverted cells showing red Dendra2 protein. Enlarged area shows the individual nuclei of photoconverted cells. Scale bar: 30 µm. (D) Regenerated fin ray at 5 dpi. Scale bar: 50 µm. (E) Newly made Dendra2 protein (green only) and previously photoconverted Dendra2 protein (green and red). Scale bar: 30 µm. Data are from *n*=3 fish.

Fig. 9. Pre-existing mural cells retain their position during regeneration, while newly formed cells require Pdgfrb signalling. Maximum intensity projections of confocal z-stacks of *TgBAC(pdgfrb:gal4ff)*[ncv24]; *Tg(UAS:GFP)*[nkuasgfp1a]; *Tg(-0.8flt1:RFP)*[hu5333] fish. (A-E) Regeneration of injured tissue (1-7 dpi). Scale bars: 50 μm for A and E. (B-D) The outlined areas show mural cells (red arrowheads, numbered) on blood vessels (cyan) in proximal (D), regenerating (C) and distal end (B) injured fin. Scale bar: 10 μm. New mural cells are marked by asterisks. Data are from *n*=3 fish. (F) Maximum intensity projections of *TgBAC(pdgfrb:mCherry)*[ncv23]; *TgBAC(col1a2:GFP)*[ca103] fish. Regeneration of injured fin (3-5 dpi). The outlined areas show *col1a2/pdgfrb* double-positive cells (marked in white, red and green). Scale bar: 10 μm. (G) Quantification of *col1a2/pdgfrb* double-positive cells in 3-5 dpi fin. Individual data points represent individual fish analysed. Unpaired *t*-test (*n*=3 animals). *P=0.0284.

stages of artery regeneration (Fig. 9F,G). However, at later stages, the number of double-positive cells diminished, indicating that cells had differentiated in either the fibroblast or mural cell lineage. Together, these findings indicate that pre-existing mural cells are not a major source of newly forming mural cells during tissue regeneration in the zebrafish fin (see summary of findings in Fig. S9). They also suggest that these cells do not serve as stem cells during the regeneration of other fin tissues.

DISCUSSION

We generated transgenic zebrafish lines to investigate blood vessel mural cell populations in the zebrafish fin during adult stages and in tissue regeneration. We discovered the existence of several distinct mural cell populations that differed with respect to their morphology and location: in fin regions proximal to the fish body, we observed mural cells ensheathing arteries, while those in distal regions extended long processes along the proximo-distal vessel axis. These

morphologies closely resemble those recently observed for subsets of mural cells on mammalian brain blood vessels (Grant et al., 2019). Furthermore, we detected differences in gene expression patterns within fin mural cells of different morphologies. All mural cells expressed *pdgfrb* and *myh11a*. This was a surprising finding, as *myh11a* was previously reported to be exclusively expressed in differentiated smooth muscle cells (Miano et al., 1994). We detected expression of *acta2* in *myh11a*-positive mural cells in proximal fin regions, suggesting the existence of smooth muscle cells that express *acta2* and *myh11a*, while mural cells in distal regions share pericyte characteristics.

Single-cell sequencing data of mouse brain tissue revealed that some pericytes also expressed *myh11*, while no *acta2* expression was detected in this cell population (Vanlandewijck et al., 2018). In line with this assessment, single-cell sequencing of mural cell populations of different mouse organs has revealed a surprising diversification of pericytes, also in respect to the expression of

components of the SMC contractile machinery, such as *myh11*, *tagln* and *acta2* (Muhl et al., 2020; Vanlandewijck et al., 2018). In organs such as the bladder or colon, pericytes expressed *tagln* and *acta2*, while in the brain and lung they did not. Therefore, the repertoire of contractile protein expression varies between pericytes and smooth muscle cell populations, as we now also show for mural cells in the fin of zebrafish. It will be of interest to investigate the expression of recently identified pericyte-specific zebrafish transgenes (Shih et al., 2021) in fin mural cells in order to better characterize the distribution of mural cells displaying smooth muscle or pericyte features.

We show that cuboidal-shaped cells that express fibroblast genes, such as *col1a2*, can give rise to mural cells in distal regions of the fin. These findings are in line with results in embryonic zebrafish, where *col1a2*-expressing cells contribute to mural cells on intersegmental blood vessels (Rajan et al., 2020). We find a similar change in gene expression from *col1a2* high to *pdgfrb* high during fin regeneration, suggesting that the lineage transformation from cells of fibroblastic origin towards the mural cell lineage is well conserved. At present it is unclear whether other cell populations can similarly contribute to the mural cell lineage, as suggested by the differential effects of mutations in *pdgfrb* on mural cells in proximal and distal fin regions. More elaborate lineage-tracing studies will be needed to address these questions.

Fin blood vessels consist of arteries and veins that run through the entirety of the fin and are connected by inter-vessel commissures, but an elaborate capillary bed is missing, in particular in distal fin regions (Huang et al., 2003; Kametani et al., 2015; Xu et al., 2014). Our blood vessel diameter measurements revealed that fin arteries become larger towards distal regions of the fin, which contrasts with other vascular beds. Of note, in these distal regions, we predominantly detect blood vessel diameter increases in *pdgfrb* mutants. Further studies will be needed to decipher the functions of fin mural cells on vascular patterning and function, and how they compare with other organs and tissues.

The finding that newly forming mural cells in the fin were not derived from pre-existing ones was surprising, as previous studies suggested that pericytes can function as mesenchymal stem cells, even though this notion was later called into question (Birbrair et al., 2017). During wound healing, several sources of pericytes, such as pre-existing pericytes or mesenchymal stem cells, are being discussed (Morikawa et al., 2019). Although a previous study showed that bone marrow-derived mesenchymal stem cells could contribute to the pericyte lineage during wound repair (Sasaki et al., 2008), definitive lineage tracing data concerning the contribution of pre-existing pericytes is still lacking. Our studies did not find significant contribution of pre-existing mural cells to other cell types within regenerating fin tissue. This supports previous lineage-tracing results in mice showing limited stem cell properties of mural cells (Guimaraes-Camboa et al., 2017). Other studies, however, showed that pericytes can give rise to scar tissue during spinal cord injury (Göritz et al., 2011). This tissue prevented axonal regrowth in mice (Dias et al., 2018). In embryonic zebrafish, progeny of *pdgfrb*-expressing mural and myoseptal cells prevented scarring during spinal cord injury and thereby promoted axon regeneration (Tsata et al., 2021). Therefore, differences in the potential of perivascular cells during tissue regeneration and or healing might exist.

In keeping with the requirement for Pdgfrb signalling during pericyte development in embryonic stages (Armulik et al., 2011), inhibition of such signalling after wounding led to impaired pericyte recruitment (Rajkumar et al., 2006). These findings, together with our work showing deficient mural cell recruitment in *pdgfrb*

mutants during tissue regeneration, underline the role of Pdgfrb signalling as a master regulator of pericyte biology in different biological settings.

We found that mural cells in proximal fin regions still formed in *pdgfrb* mutants, while at the same time displaying a morphology distinct from perivascular cells in distal regions. This might suggest that distinct signalling pathways controlling mural cell recruitment and differentiation exist in different areas of the fin. We now find activation of the Notch signalling pathway only in mural cells in distal fin regions, supporting this hypothesis. These observations might further indicate separate embryonic origins for mural cells along the proximo-distal fin axis. Alternatively, distally located perivascular cells might give rise to proximal mural cell populations in wild-type settings, as suggested by a recent study investigating smooth muscle cell development in coronary arteries (Volz et al., 2015). Here, pericytes located on distal vessel branches are a precursor population for smooth muscle cells. In *pdgfrb* mutants, this route of distal to proximal differentiation would be compromised, leading to the activation of alternative sources for mural cells not normally used in wild-type fish. Detailed linage-tracing studies in combination with single-cell sequencing approaches will be needed to answer these questions and to determine how they relate to mural cells in other tissues and organisms.

MATERIALS AND METHODS
Zebrafish husbandry and strains
Zebrafish embryos were maintained in 1×E3 under standard husbandry conditions for 5 days in an incubator at 28.5°C. After 5 days, the embryos were transferred to embryo tanks in the zebrafish facility, where they were raised until adulthood. Previously described zebrafish lines were *Tg(0.8flt1:RFP)*[hu5333] (Bussmann et al., 2010), *TgBAC(pdgfrb:citrine)*[s1010] (Vanhollebeke et al., 2015), *TgBAC(pdgfrb:mCherry)*[ncv23] (Ando et al., 2016), *TgBAC(pdgfrb:gal4ff)*[ncv24] (Ando et al., 2016), *Tg(kdrl:TagBFP)*[mu293] (Matsuoka et al., 2016), *pdgfrb*[um148] (Kok et al., 2015), *TgBAC(col1a2:GFP)*[ca103] (Ma et al., 2018), *Tg(acta2:mCherry)*[ca8] (Whitesell et al., 2014), *Tg(TP1bglob:VenusPEST)*[s940] (Ninov et al., 2012), *Tg(TP1bglob:H2BmCherry)*[s939] (Ninov et al., 2012) and *Tg3(fli1:LIFEACT-EGFP)*[mu240] (Hamm et al., 2016). All animal experiments were performed in compliance with the relevant laws and institutional guidelines, and were approved by local animal ethics committees of the Landesamt für Natur, Umwelt und Verbraucherschutz Nordrhein-Westfalen.

Generation of transgenic lines
Transgenic lines were generated using Bacterial artificial chromosome (BAC) recombineering. To generate the *TgBAC(myh11a:YFP)*[mu125] and *TgBAC(pdgfrb:H2B-dendra2)*[mu158], the start codons of *myh11a* or *pdgfrb* in BAC clone CH73-223E22 or CH1073-606I16 were replaced with YFP or H2B-Dendra2 cassette using Red/ET recombineering (GeneBridges). The YFP cassette was amplified by PCR from pCS2+Citrine_kanR with the primers myh11a _HA1_citrine_fw (5′-ttatcaatcagtttttctccttaaatttgcagttgtct-taacccagcaccACCATGGTGAGCAAGGGCGAGGAG-3′) and myh11a_-HA2_kanR_rev (5′-tctttgtccgtgaaaaggaatttctcatcatcgctcaagccttctcttcgtTCA-GAAGAACTCGTCAAGAAGGCG-3′); homology to the BAC vector is depicted in lowercase throughout. iTol2_amp cassette was inserted into the vector back bone using a construct amplified with primers pTarBAC_i-Tol2_fw (5′-gcgtaagcggggcacatttcattacctctttctccgcacccgacatagatCCCTGC-TCGAGCCGGGCCCAAGTG-3′) and pTarBAC_iTol2_rev (5′-gcgggg-catgactattggcgcgccgatcgatccttaattaagtctactaATTATGATCCTCTAGATCA-GATC-3′). The H2B-Dendra2 cassette was amplified by PCR from pCS2+H2B-Dendra2_kanR with primers Pdgfrb_HA1_dendra2_fw (5′-tgttgtttttctctccgtctgcagtgttgaatgtgtcctgctctagaagaaCCACCATGCCAGAGC-CAGCGAA) and Pdgfrb_HA1_dendra2_rev (5′-ttgtgatagcagtgaatagga-agtggatgcggctgatggtcgaactcttTCAGAAGAACTCGTCAAGAAGGCG-3′). The iTol2_amp cassette was inserted into the vector back bone using a

construct amplified with primers pCC1FOS_ iTol2 _fw (5′-tctctgttttt-gtccgtggaatgaacaatggaagtccgagctcatcgctaCCCTGCTCGAGCCGGGCCC-AAGTG-3′) and pCC1FOS_ iTol2 _rev (5′-cgacacccgccaacacccgctgac-gcgaaccccttgcggccgcatcgaatATTATGATCCTCTAGATCAGATC).   BAC DNA was purified using Midiprep (Invitrogen) on the day of injection. A cocktail of 100 pg BAC DNA and 50 pg of tol2 transposase mRNA per embryo was injected into wild-type embryos.

Bone regeneration and fin amputation
Adult zebrafish were anaesthetized with 0.02% tricaine and transferred to a Petri plate. Bone resection was performed by removing a piece of bone ray enclosing an artery in the third or fourth fin ray of the dorsal or ventral lobe, using a scalpel. For fin amputation, ∼50% of the fin was amputated and the third fin ray from the dorsal or ventral lobe was used for analysis. The injured fish were kept in individual tanks until experiments were carried out.

Confocal microscopy
Larvae or amputated fins were embedded in 1% low melting point agarose. Fluorescent confocal images were acquired using a Zeiss LSM 780/880 (objective lens: 20× Plan Apo NA 0.80 or 40× LD C Apochromat NA 1.10) or Leica SP8 (objective lens: HC PL Fluotar 20×/0.50 or HCX APO L 63).

Photoconversion and lineage tracing
For lineage tracing of cuboidal cells, we performed photoconversion in the distal regions of the juvenile fin. The anesthetized larvae were embedded in 0.75% agarose containing 0.02% tricaine. Cuboidal-shaped cells were identified based on their morphology. We then chose regions in the fin that contained only cuboidal-shaped cells and were devoid of cell with elongated mural cell morphologies. We marked these regions containing between 5 and 20 cells in the Zeiss Zen software. The selected cells were exposed to 8% of 405 nm laser excitation wavelength with 40 iterations for 25 cycles. Immediately after photoconversion, we imaged fins to determine the number of photoconverted cells. This image also served as 0 dpc. The larvae were removed from the glass plates and placed in fresh E3 medium with no light exposure and reimaged after 5 days. For lineage tracing of photoconverted Dendra2 cells during adult fin regeneration, bone resection was performed in adult fins; at 12 h post-injury, anesthetized fish were transferred to glass plates and immobilized with 1.5% agarose. To keep fish sedated, E3 media containing 0.02% tricaine was added to the glass plate and the agarose around the gills, heart and mouth of the fish was carefully removed. Photoconversion was performed by selecting regions in Zeiss Zen, around the resected bone with 10% of 405 nm laser with 40 iterations for 25 cycles. After photoconversion, fish were placed in individual tanks containing fresh E3. To speed up recovery, we used a pipette to transfer E3 to the mouth and gills of the fish. Tanks containing photoconverted fish were kept in dark with minimal exposure to light provided only during feeding. For photoconversion of Kaede-expressing cells, amputated fin segments were embedded in agarose and photoconverted using a 405 nm laser with laser power of 8% and 30 iterations. Images for native or photoconverted Dendra2 and Kaede were acquired using laser settings for EGFP and RFP. For repetitive imaging, adult fish were immobilized on glass plates as described before and recovered after every session.

Image processing and analysis
Acquired images were stitched using Zeiss ZEN software or Leica LAS-X. Imaris software (Bitplane) was used to generate maximum intensity projections. The dimensions of cuboidal and mural cells with protrusions were determined by measuring their length and width. The distribution of mural cells that wrap or extend protrusions was quantified using Imaris software. Artery diameter along the proximal distal axis was calculated by measuring vessel diameter in at least ten regions for each of the four segments. Data were analysed using Prism 9 (Graphpad) and graphs were plotted as mean±s.d. $P<0.05$ was considered statistically significant. ImageJ (NIH) was used to generate monochrome images of different fluorophores and to calculate fluorescent intensity. Adobe Illustrator software was used to compile images.

Fluorescence activated cell sorting and qPCR
Caudal fins of 4 wpf zebrafish were amputated and washed twice with 1× HBSS (Gibco, 14185052) in a 1.5 ml microcentrifuge tube. Amputated fins were treated with TrypLE Express Enzyme (1×) (Gibco, 12604013) at 37°C for 30 min with gentle agitation. TrypLE-treated samples were centrifuged at 500 g for 5 min at 4°C, and the supernatant was carefully removed and discarded. The samples were further treated with 1 ml of 0.50 mg/ml of Liberase DL (Roche, 5401160001) in 1× HBSS at 37°C for 30 min with agitation to obtain a single-cell suspension. Dissociated cells were pelleted by centrifugation at 350 g for 5 min at 4°C. The cell pellet was resuspended in 1× HBSS buffer and centrifuged twice. The cells were resuspended in 500 μl of 1× HBSS and passed through a 40 μm nylon filter. Fluorescence-activated cell sorting (FACS) was performed for *pdgfrb*- (RFP), *myh11a*-(YFP) and RFP/YFP-expressing mural cells (RFP/YFP). Sorted cells were collected in RLT buffer followed by RNA isolation using the RNeasy Micro kit (Qiagen, 74004), and cDNA synthesis was performed using the iScript cDNA Synthesis Kit (BioRad, 1708891). qPCR was performed using Power SYBR Green PCR Master Mix (Applied Biosystems, 4367659). The ddCt method was used to calculate relative expression using RPL13a as endogenous control, dCt data were used to perform statistical analysis. Primer sequences are listed in Table S1.

Competing interests
The authors declare no competing or financial interests.

Author contributions
Conceptualization: E.V.L., A.F.S.; Validation: E.V.L.; Formal analysis: E.V.L.; Investigation: E.V.L., R.J.F.; Resources: E.V.L., J.B., N.D.L.; Data curation: E.V.L.; Writing - original draft: E.V.L.; Writing - review & editing: E.V.L., J.B., J.D.A., A.F.S.; Visualization: E.V.L.; Supervision: J.D.A., A.F.S.; Project administration: A.F.S.; Funding acquisition: J.D.A., A.F.S.

Peer review history
The peer review history is available online at https://journals.biologists.com/dev/article-lookup/doi/10.1242/dev.199640.

References
Alunni, A. and Bally-Cuif, L. (2016). A comparative view of regenerative neurogenesis in vertebrates. *Development* 143, 741-753. doi:10.1242/dev.122796

Ando, K., Fukuhara, S., Izumi, N., Nakajima, H., Fukui, H., Kelsh, R. N. and Mochizuki, N. (2016). Clarification of mural cell coverage of vascular endothelial cells by live imaging of zebrafish. *Development* 143, 1328-1339. doi:10.1242/dev.132654

Ando, K., Shih, Y.-H., Ebarasi, L., Grosse, A., Portman, D., Chiba, A., Mattonet, K., Gerri, C., Stainier, D. Y. R., Mochizuki, N. et al. (2021). Conserved and context-dependent roles for pdgfrb signaling during zebrafish vascular mural cell development. *Dev. Biol.* 479, 11-22. doi:10.1016/j.ydbio.2021.06.010

Ansell, D. M. and Izeta, A. (2015). Pericytes in wound healing: friend or foe? *Exp. Dermatol.* 24, 833-834. doi:10.1111/exd.12782

Armulik, A., Genové, G. and Betsholtz, C. (2011). Pericytes: developmental, physiological, and pathological perspectives, problems, and promises. *Dev. Cell* 21, 193-215. doi:10.1016/j.devcel.2011.07.001

Birbrair, A., Borges, I. D. T., Gilson Sena, I. F., Almeida, G. G., da Silva Meirelles, L., Goncalves, R., Mintz, A. and Delbono, O. (2017). How plastic are pericytes? *Stem Cells Dev.* 26, 1013-1019. doi:10.1089/scd.2017.0044

DEVELOPMENT

Bussmann, J., Bos, F. L., Urasaki, A., Kawakami, K., Duckers, H. J. and Schulte-Merker, S. (2010). Arteries provide essential guidance cues for lymphatic endothelial cells in the zebrafish trunk. *Development* **137**, 2653-2657. doi:10.1242/dev.048207

Carmeliet, P. (2005). Angiogenesis in life, disease and medicine. *Nature* **438**, 932-936. doi:10.1038/nature04478

Chavez, M. N., Aedo, G., Fierro, F. A., Allende, M. L. and Egana, J. T. (2016). Zebrafish as an emerging model organism to study angiogenesis in development and regeneration. *Front. Physiol.* **7**, 56. doi:10.3389/fphys.2016.00056

Crisan, M., Yap, S., Casteilla, L., Chen, C.-W., Corselli, M., Park, T. S., Andriolo, G., Sun, B., Zheng, B., Zhang, L. et al. (2008). A perivascular origin for mesenchymal stem cells in multiple human organs. *Cell Stem Cell* **3**, 301-313. doi:10.1016/j.stem.2008.07.003

Crosby, J. R., Seifert, R. A., Soriano, P. and Bowen-Pope, D. F. (1998). Chimaeric analysis reveals role of Pdgf receptors in all muscle lineages. *Nat. Genet.* **18**, 385-388. doi:10.1038/ng0498-385

de Wit, L., Fang, J., Neef, K., Xiao, J., P, A. D., Schiffelers, R. M., Lei, Z. and Sluijter, J. P. G. (2020). Cellular and molecular mechanism of cardiac regeneration: a comparison of newts, zebrafish, and mammals. *Biomolecules* **10**, 1204. doi:10.3390/biom10091204

Dellavalle, A., Sampaolesi, M., Tonlorenzi, R., Tagliafico, E., Sacchetti, B., Perani, L., Innocenzi, A., Galvez, B. G., Messina, G., Morosetti, R. et al. (2007). Pericytes of human skeletal muscle are myogenic precursors distinct from satellite cells. *Nat. Cell Biol.* **9**, 255-267. doi:10.1038/ncb1542

Dellavalle, A., Maroli, G., Covarello, D., Azzoni, E., Innocenzi, A., Perani, L., Antonini, S., Sambasivan, R., Brunelli, S., Tajbakhsh, S. et al. (2011). Pericytes resident in postnatal skeletal muscle differentiate into muscle fibres and generate satellite cells. *Nat. Commun.* **2**, 499. doi:10.1038/ncomms1508

Dias, D. O., Kim, H., Holl, D., Werne Solnestam, B., Lundeberg, J., Carlen, M., Goritz, C. and Frisen, J. (2018). Reducing pericyte-derived scarring promotes recovery after spinal cord injury. *Cell* **173**, 153-165.e22. doi:10.1016/j.cell.2018.02.004

DiPietro, L. A. (2013). Angiogenesis and scar formation in healing wounds. *Curr. Opin. Rheumatol.* **25**, 87-91. doi:10.1097/BOR.0b013e32835b13b6

DiPietro, L. A. (2016). Angiogenesis and wound repair: when enough is enough. *J. Leukoc. Biol.* **100**, 979-984. doi:10.1189/jlb.4MR0316-102R

Dore-Duffy, P., Katychev, A., Wang, X. and Van Buren, E. (2006). CNS microvascular pericytes exhibit multipotential stem cell activity. *J. Cereb. Blood Flow Metab.* **26**, 613-624. doi:10.1038/sj.jcbfm.9600272

Eilken, H. M., Dieguez-Hurtado, R., Schmidt, I., Nakayama, M., Jeong, H. W., Arf, H., Adams, S., Ferrara, N. and Adams, R. H. (2017). Pericytes regulate VEGF-induced endothelial sprouting through VEGFR1. *Nat. Commun.* **8**, 1574. doi:10.1038/s41467-017-01738-3

Eming, S. A., Martin, P. and Tomic-Canic, M. (2014). Wound repair and regeneration: mechanisms, signaling, and translation. *Sci. Transl. Med.* **6**, 265-266. doi:10.1126/scitranslmed.3009337

Erickson, J. R. and Echeverri, K. (2018). Learning from regeneration research organisms: the circuitous road to scar free wound healing. *Dev. Biol.* **433**, 144-154. doi:10.1016/j.ydbio.2017.09.025

Fortuna, V., Pardanaud, L., Brunet, I., Ola, R., Ristori, E., Santoro, M. M., Nicoli, S. and Eichmann, A. (2015). Vascular mural cells promote noradrenergic differentiation of embryonic sympathetic neurons. *Cell Rep.* **11**, 1786-1796. doi:10.1016/j.celrep.2015.05.028

Gabbiani, G., Schmid, E., Winter, S., Chaponnier, C., de Ckhastonay, C., Vandekerckhove, J., Weber, K. and Franke, W. W. (1981). Vascular smooth muscle cells differ from other smooth muscle cells: predominance of vimentin filaments and a specific alpha-type actin. *Proc. Natl. Acad. Sci. USA* **78**, 298-302. doi:10.1073/pnas.78.1.298

Gaengel, K., Genové, G., Armulik, A. and Betsholtz, C. (2009). Endothelial-mural cell signaling in vascular development and angiogenesis. *Arterioscler. Thromb. Vasc. Biol.* **29**, 630-638. doi:10.1161/ATVBAHA.107.161521

González-Rosa, J. M., Burns, C. E. and Burns, C. G. (2017). Zebrafish heart regeneration: 15 years of discoveries. *Regeneration (Oxf)* **4**, 105-123. doi:10.1002/reg2.83

Göritz, C., Dias, D. O., Tomilin, N., Barbacid, M., Shupliakov, O. and Frisén, J. (2011). A pericyte origin of spinal cord scar tissue. *Science* **333**, 238-242. doi:10.1126/science.1203165

Grant, R. I., Hartmann, D. A., Underly, R. G., Berthiaume, A.-A., Bhat, N. R. and Shih, A. Y. (2019). Organizational hierarchy and structural diversity of microvascular pericytes in adult mouse cortex. *J. Cereb. Blood Flow Metab.* **39**, 411-425. doi:10.1177/0271678X17732229

Guimaraes-Camboa, N., Cattaneo, P., Sun, Y., Moore-Morris, T., Gu, Y., Dalton, N. D., Rockenstein, E., Masliah, E., Peterson, K. L., Stallcup, W. B. et al. (2017). Pericytes of multiple organs do not behave as mesenchymal stem cells in vivo. *Cell Stem Cell* **20**, 345-359.e45. doi:10.1016/j.stem.2016.12.006

Hall, C. N., Reynell, C., Gesslein, B., Hamilton, N. B., Mishra, A., Sutherland, B. A., O'Farrell, F. M., Buchan, A. M., Lauritzen, M. and Attwell, D. (2014). Capillary pericytes regulate cerebral blood flow in health and disease. *Nature* **508**, 55-60. doi:10.1038/nature13165

Hamm, M. J., Kirchmaier, B. C. and Herzog, W. (2016). Sema3d controls collective endothelial cell migration by distinct mechanisms via Nrp1 and PlxnD1. *J. Cell Biol.* **215**, 415-430. doi:10.1083/jcb.201603100

Hellstrom, M., Kalen, M., Lindahl, P., Abramsson, A. and Betsholtz, C. (1999). Role of PDGF-B and PDGFR-beta in recruitment of vascular smooth muscle cells and pericytes during embryonic blood vessel formation in the mouse. *Development* **126**, 3047-3055. doi:10.1242/dev.126.14.3047

Hellstrom, M., Gerhardt, H., Kalén, M., Li, X., Eriksson, U., Wolburg, H. and Betsholtz, C. (2001). Lack of pericytes leads to endothelial hyperplasia and abnormal vascular morphogenesis. *J. Cell Biol.* **153**, 543-553. doi:10.1083/jcb.153.3.543

Holm, A., Heumann, T. and Augustin, H. G. (2018). Microvascular mural cell organotypic heterogeneity and functional plasticity. *Trends Cell Biol.* **28**, 302-316. doi:10.1016/j.tcb.2017.12.002

Huang, C.-C., Lawson, N. D., Weinstein, B. M. and Johnson, S. L. (2003). reg6 is required for branching morphogenesis during blood vessel regeneration in zebrafish caudal fins. *Dev. Biol.* **264**, 263-274. doi:10.1016/j.ydbio.2003.08.016

Kametani, Y., Chi, N. C., Stainier, D. Y. R. and Takada, S. (2015). Notch signaling regulates venous arterialization during zebrafish fin regeneration. *Genes Cells* **20**, 427-438. doi:10.1111/gtc.12234

Kazlauskas, A. (2017). PDGFs and their receptors. *Gene* **614**, 1-7. doi:10.1016/j.gene.2017.03.003

Kok, F. O., Shin, M., Ni, C.-W., Gupta, A., Grosse, A. S., van Impel, A., Kirchmaier, B. C., Peterson-Maduro, J., Kourkoulis, G., Male, I. et al. (2015). Reverse genetic screening reveals poor correlation between morpholino-induced and mutant phenotypes in zebrafish. *Dev. Cell* **32**, 97-108. doi:10.1016/j.devcel.2014.11.018

Langen, U. H., Ayloo, S. and Gu, C. (2019). Development and cell biology of the blood-brain barrier. *Annu. Rev. Cell Dev. Biol.* **35**, 591-613. doi:10.1146/annurev-cellbio-100617-062608

Li, L., Miano, J. M., Cserjesi, P. and Olson, E. N. (1996). SM22α, a marker of adult smooth muscle, is expressed in multiple myogenic lineages during embryogenesis. *Circ. Res.* **78**, 188-195. doi:10.1161/01.RES.78.2.188

Lindahl, P., Johansson, B. R., Levéen, P. and Betsholtz, C. (1997). Pericyte loss and microaneurysm formation in PDGF-B-deficient mice. *Science* **277**, 242-245. doi:10.1126/science.277.5323.242

Ma, R. C., Jacobs, C. T., Sharma, P., Kocha, K. M. and Huang, P. (2018). Stereotypic generation of axial tenocytes from bipartite sclerotome domains in zebrafish. *PLoS Genet.* **14**, e1007775. doi:10.1371/journal.pgen.1007775

Matsuoka, R. L., Marass, M., Avdesh, A., Helker, C. S. M., Maischein, H.-M., Grosse, A. S., Kaur, H., Lawson, N. D., Herzog, W. and Stainier, D. Y. (2016). Radial glia regulate vascular patterning around the developing spinal cord. *eLife* **5**, e20253. doi:10.7554/eLife.20253

McDonald, A. I., Shirali, A. S., Aragón, R., Ma, F., Hernandez, G., Vaughn, D. A., Mack, J. J., Lim, T. Y., Sunshine, H., Zhao, P. et al. (2018). Endothelial regeneration of large vessels is a biphasic process driven by local cells with distinct proliferative capacities. *Cell Stem Cell* **23**, 210-225.e16. doi:10.1016/j.stem.2018.07.011

Miano, J. M., Cserjesi, P., Ligon, K. L., Periasamy, M. and Olson, E. N. (1994). Smooth muscle myosin heavy chain exclusively marks the smooth muscle lineage during mouse embryogenesis. *Circ. Res.* **75**, 803-812. doi:10.1161/01.RES.75.5.803

Morikawa, S., Iribar, H., Gutiérrez-Rivera, A., Ezaki, T. and Izeta, A. (2019). Pericytes in cutaneous wound healing. *Adv. Exp. Med. Biol.* **1147**, 1-63. doi:10.1007/978-3-030-16908-4_1

Muhl, L., Genové, G., Leptidis, S., Liu, J., He, L., Mocci, G., Sun, Y., Gustafsson, S., Buyandelger, B., Chivukula, I. V. et al. (2020). Single-cell analysis uncovers fibroblast heterogeneity and criteria for fibroblast and mural cell identification and discrimination. *Nat. Commun.* **11**, 3953. doi:10.1038/s41467-020-17740-1

Ninov, N., Borius, M. and Stainier, D. Y. R. (2012). Different levels of Notch signaling regulate quiescence, renewal and differentiation in pancreatic endocrine progenitors. *Development* **139**, 1557-1567. doi:10.1242/dev.076000

Pfeiffer, T., Li, Y. and Attwell, D. (2021). Diverse mechanisms regulating brain energy supply at the capillary level. *Curr. Opin. Neurobiol.* **69**, 41-50. doi:10.1016/j.conb.2020.12.010

Poss, K. D. (2010). Advances in understanding tissue regenerative capacity and mechanisms in animals. *Nat. Rev. Genet.* **11**, 710-722. doi:10.1038/nrg2879

Rajan, A. M., Ma, R. C., Kocha, K. M., Zhang, D. J. and Huang, P. (2020). Dual function of perivascular fibroblasts in vascular stabilization in zebrafish. *PLoS Genet.* **16**, e1008800. doi:10.1371/journal.pgen.1008800

Rajkumar, V. S., Shiwen, X., Bostrom, M., Leoni, P., Muddle, J., Ivarsson, M., Gerdin, B., Denton, C. P., Bou-Gharios, G., Black, C. M. et al. (2006). Platelet-derived growth factor-beta receptor activation is essential for fibroblast and pericyte recruitment during cutaneous wound healing. *Am. J. Pathol.* **169**, 2254-2265. doi:10.2353/ajpath.2006.060196

Rodrigues, M., Kosaric, N., Bonham, C. A. and Gurtner, G. C. (2019). Wound healing: a cellular perspective. *Physiol. Rev.* **99**, 665-706. doi:10.1152/physrev.00067.2017

DEVELOPMENT

Santoro, M. M., Pesce, G. and Stainier, D. Y. (2009). Characterization of vascular mural cells during zebrafish development. *Mech. Dev.* **126**, 638-649. doi:10.1016/j.mod.2009.06.1080

Sasaki, M., Abe, R., Fujita, Y., Ando, S., Inokuma, D. and Shimizu, H. (2008). Mesenchymal stem cells are recruited into wounded skin and contribute to wound repair by transdifferentiation into multiple skin cell type. *J. Immunol.* **180**, 2581-2587. doi:10.4049/jimmunol.180.4.2581

Sehring, I. M. and Weidinger, G. (2020). Recent advancements in understanding fin regeneration in zebrafish. *Wiley Interdiscip. Rev. Dev. Biol.* **9**, e367. doi:10.1002/wdev.367

Shih, Y.-H., Portman, D., Idrizi, F., Grosse, A. and Lawson, N. D. (2021). Integrated molecular analysis identifies a conserved pericyte gene signature in zebrafish. *Development* **148**, dev200189. doi:10.1242/dev.200189

Sinha, S. and Santoro, M. M. (2018). New models to study vascular mural cell embryonic origin: implications in vascular diseases. *Cardiovasc. Res.* **114**, 481-491. doi:10.1093/cvr/cvy005

Stratman, A. N., Pezoa, S. A., Farrelly, O. M., Castranova, D., Dye, L. E., III, Butler, M. G., Sidik, H., Talbot, W. S. and Weinstein, B. M. (2017). Interactions between mural cells and endothelial cells stabilize the developing zebrafish dorsal aorta. *Development* **144**, 115-127. doi:10.1242/dev.143131

Tanaka, E. M. (2016). The molecular and cellular choreography of appendage regeneration. *Cell* **165**, 1598-1608. doi:10.1016/j.cell.2016.05.038

Tanaka, E. M. and Reddien, P. W. (2011). The cellular basis for animal regeneration. *Dev. Cell* **21**, 172-185. doi:10.1016/j.devcel.2011.06.016

Tang, W., Zeve, D., Suh, J. M., Bosnakovski, D., Kyba, M., Hammer, R. E., Tallquist, M. D. and Graff, J. M. (2008). White fat progenitor cells reside in the adipose vasculature. *Science* **322**, 583-586. doi:10.1126/science.1156232

Teichert, M., Milde, L., Holm, A., Stanicek, L., Gengenbacher, N., Savant, S., Ruckdeschel, T., Hasanov, Z., Srivastava, K., Hu, J. et al. (2017). Pericyte-expressed Tie2 controls angiogenesis and vessel maturation. *Nat. Commun.* **8**, 16106. doi:10.1038/ncomms16106

Tonnesen, M. G., Feng, X. and Clark, R. A. F. (2000). Angiogenesis in wound healing. *J. Investig. Dermatol. Symp. Proc.* **5**, 40-46. doi:10.1046/j.1087-0024.2000.00014.x

Tsata, V., Mollmert, S., Schweitzer, C., Kolb, J., Mockel, C., Bohm, B., Rosso, G., Lange, C., Lesche, M., Hammer, J. et al. (2021). A switch in pdgfrb(+) cell-derived ECM composition prevents inhibitory scarring and promotes axon regeneration in the zebrafish spinal cord. *Dev. Cell* **56**, 509-524.e9. doi:10.1016/j.devcel.2020.12.009

Tu, S. and Johnson, S. L. (2011). Fate restriction in the growing and regenerating zebrafish fin. *Dev. Cell* **20**, 725-732. doi:10.1016/j.devcel.2011.04.013

Vanhollebeke, B., Stone, O. A., Bostaille, N., Cho, C., Zhou, Y., Maquet, E., Gauquier, A., Cabochette, P., Fukuhara, S., Mochizuki, N. et al. (2015). Tip cell-specific requirement for an atypical Gpr124- and Reck-dependent Wnt/beta-catenin pathway during brain angiogenesis. *eLife* **4**, e06489. doi:10.7554/eLife.06489

Vanlandewijck, M., He, L., Mäe, M. A., Andrae, J., Ando, K., Del Gaudio, F., Nahar, K., Lebouvier, T., Laviña, B., Gouveia, L. et al. (2018). A molecular atlas of cell types and zonation in the brain vasculature. *Nature* **554**, 475-480. doi:10.1038/nature25739

Volz, K. S., Jacobs, A. H., Chen, H. I., Poduri, A., McKay, A. S., Riordan, D. P., Kofler, N., Kitajewski, J., Weissman, I. and Red-Horse, K. (2015). Pericytes are progenitors for coronary artery smooth muscle. *eLife* **4**, e10036. doi:10.7554/eLife.10036

Wan, J. and Goldman, D. (2016). Retina regeneration in zebrafish. *Curr. Opin. Genet. Dev.* **40**, 41-47. doi:10.1016/j.gde.2016.05.009

Wang, Y., Pan, L., Moens, C. B. and Appel, B. (2014). Notch3 establishes brain vascular integrity by regulating pericyte number. *Development* **141**, 307-317. doi:10.1242/dev.096107

Whitesell, T. R., Kennedy, R. M., Carter, A. D., Rollins, E.-L., Georgijevic, S., Santoro, M. M. and Childs, S. J. (2014). An alpha-smooth muscle actin (acta2/alphasma) zebrafish transgenic line marking vascular mural cells and visceral smooth muscle cells. *PLoS ONE* **9**, e90590. doi:10.1371/journal.pone.0090590

Xiang, M. S. and Kikuchi, K. (2016). Endogenous mechanisms of cardiac regeneration. *Int. Rev. Cell Mol. Biol.* **326**, 67-131. doi:10.1016/bs.ircmb.2016.04.002

Xu, C., Hasan, S. S., Schmidt, I., Rocha, S. F., Pitulescu, M. E., Bussmann, J., Meyen, D., Raz, E., Adams, R. H. and Siekmann, A. F. (2014). Arteries are formed by vein-derived endothelial tip cells. *Nat. Commun.* **5**, 5758. doi:10.1038/ncomms6758